Postprint of a paper published as Marine Structures 80 (2021) 103093

Real time prediction of operational safety limits for dynamic positioning of an FPSO in a Deepwater Artificial Seabed system

Yue Han[a], Xingwei Zhen[a,*], Torgeir Moan[b], Yi Huang[a]

a School of Naval Architecture and Ocean Engineering, Dalian University of Technology (DUT), NO-116024 Dalian, China

b Department of Marine Technology and Centre for Autonomous Marine Operations and Systems (AMOS), Norwegian University of Science and Technology (NTNU), Trondheim 7491, Norway

Abstract

Aiming to overcome the limitations of conventional offshore field development concepts (dry tree or subsea tree) for petroleum production in ultra-deep water, a new alternative offshore field development solution, termed as Deepwater Artificial Seabed (DAS) system, is proposed. The DAS system works in concert with dynamic positioning (DP) floaters, such as dynamically positioned Floating Production, Storage and Offloading (FPSO) vessels. Rather than relying on the passive mooring system, the DP maintains the reliable position of the FPSO with steering and propulsion units. Nonetheless, critical DP failures, which has potential to cause the drift-off scenario for the FPSO, and poses a serious threat to the structural safety of the DAS system. Therefore, it is crucial to establish operational limits for the DP FPSO to prevent such accidents. In this study, a 3-phase probabilistic modelling methodology is proposed to predict safety limits for the operation of the DP FPSO. A surrogate model is established by the Support Vector Machine (SVM) algorithm so as to decrease the computational cost due to the generation of large statistical samples. The statistical distribution of the operational safety limits of FPSO is simulated by the successive approximations through the fully-coupled drift-off analysis. The accuracy of the proposed methodology is verified by a series of mathematical tests. In order to validate the effectiveness of the methodology, the safety limit prediction of the FPSO for the DAS system is taken as a case study. The critical positions of the FPSO are predicted in real time and provides ample time and information for operators' decision-making by the visualization of the safe moving range of the FPSO. The study contributes to the safety control of DP operations on floating production units in an efficient manner.

Key words: Dynamic positioning; artificial seabed; drift-off; operational safety limit; surrogate model

* Corresponding author.
E-mail address: zhenxingwei@dlut.edu.cn (X.W. Zhen).

1. Introduction

1.1. Background and research motivation

With fewer remaining easy-to-access oil and gas fields, the offshore petroleum industry has moved into deep and ultra-deep water. However, some deep-water oil and gas fields are evaluated to have no commercial value using existing conventional oil field development approaches [1], especially in a low oil price environment. These conventional oil field development approaches mainly include dry tree units or subsea developments, or a combination of both [2]. A new alternative offshore field development solution, termed as the Deepwater Artificial Seabed (DAS) system [3-6], is proposed to overcome the technical and commercial limitations of the current offshore field development concepts for petroleum production in ultra-deep water. Fig. 1 depicts the general arrangement of the DAS system. In contrast to the geological seabed, the artificial seabed, which is positioned certain distances below Mean Water Level (MWL) to minimize the adverse effects of the harsh surface environment, is established to support the shallow water rated well completion equipment and technology for the development of large oil and gas fields in ultra-deep water. The DAS system works in concert with dynamic positioning (DP) floaters, such as dynamically positioned Floating Production, Storage and Offloading (FPSO) vessels.

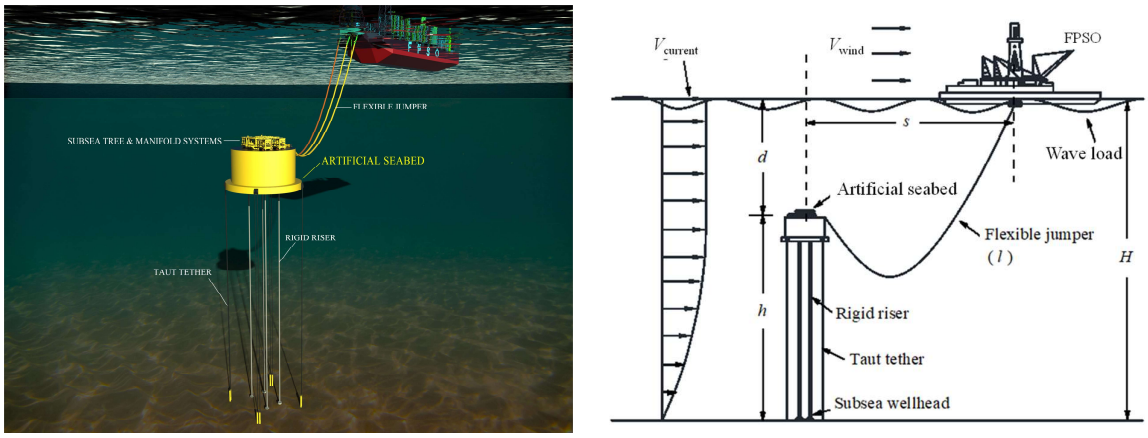

Fig. 1. Arrangement of the DAS system.

Rather than relying on the passive mooring system, DP system maintains the reliable position of FPSO with power, thruster and control systems. Nonetheless, critical DP failures, which has the potential to cause the drift-off scenario for FPSO [7, 8], and poses a significant threat to the structural safety of the DAS system. In worst case, the situation may escalate into a serious subsurface blowout and further result in a significant downtime of the petroleum production and financial losses. Therefore, emergency quick disconnection (EQD), which is an important safety barrier [7] to prevent accidents due to the excessive drift of FPSO, should be activated to disconnect the DAS system and FPSO. Besides, emergency disconnection sequence (EDS) operations are required to achieve the EQD activation. The point of disconnection as well as the associated preparation and initiation points for EDS, defined as physical, red and yellow limits respectively, are critical to the success of EQD. Therefore, it is of great importance

to predict the operational safety limits of FPSO so as to provide operators ample time and information to ensure disconnection is completed before any damage occurs to the system.

The increasing DP failure incidents provoke the stakeholders' awareness of the importance of establishing the operational safety limits. Well Specific Operating Guidelines (WSOG), which is the main tool for the safety evaluation and decision making in DP operations [9], specifies that the safety limits of mobile offshore drilling unit (MODU) should be determined prior to operation. In accordance with DNV-RP-E307 [10], the safety limit should be extracted from the MODU's riser drift-off analysis for a variety of conditions, including one-year return conditions, ten-year winter storm return conditions and where appropriate, specific return conditions such as ten-year loop current conditions. However, the original estimation, which disregards non-extreme sea states and the variation of environmental loads, would be would be conservative and not of sufficient accuracy for practical applications. Therefore, a real-time prediction methodology that takes into account the variation in environmental loads is on demand to achieve a more accurate operational safety limit.

1.2. Relevant works and objective

The existing approaches for safety limit determination mainly focus on MODU, but remarkably little attention has been paid on DP FPSO in the production phase even though there is a high position loss potential due to the DP failure. The simplest approach is to take a certain percentage of the water depth as the safety limit [11]. It is an empirical estimation and disregards the mechanical characteristics of the riser system and vessel motion, and hence lacks accuracy. Rustad et al. [12] recommend that the riser analysis should be conducted to determine the safety limit using a finite element program, such as Reflex, ABARQUS and Orcaflex. But the effects of the vessel motion and the associated time to activate EQD are disregarded. Bhalla and Cao [13] propose a non-coupled analysis approach to incorporate the effect of the vessel motion on the riser system. In their work, the vessel's trajectory over time, which should be obtained by a simulation of the vessel motion, is taken as the top boundary condition for the riser analysis. However, this approach disregards the effects of the riser system on the vessel motion, such as the drag and inertia of riser, as well as the recovery force of riser on the vessel. In view of this, some studies [14-16] propose a fully-coupled analysis approach to consider the interactions between the riser system and vessel, thus improving the accuracy of result.

However, aforementioned approaches disregard the variation of environmental loads over time. It is necessary to update the safety limit in real time with the variation of environmental loads. Gjerde and Chen [17] propose a probabilistic methodology based on the Monte Carlo (MC) simulation to predict the statistical distribution of the safety limit. But it is also difficult to apply this methodology to the real-time DP operation since numerous numerical simulations are required to calculate large statistical samples. The computational cost due to frequent numerical simulation will also result in a delay of information transmission to decision makers.

It is recognized that a new technique to reduce the computational cost is to use surrogate models [18, 19]. The

surrogate model approximates the data which needs to be simulated with the numerical model and thus reduce the calculation cost of the sample set. Therefore, the objective of this study is to propose a 3-phase probabilistic modelling methodology to predict the operational safety limits of the DP FPSO, taking into account the variation in environmental loads. The proposed methodology is based on integrating the surrogate model and mechanical model with the probabilistic methodology to reduce the computational expense. This methodology aims at predicting the critical situation of the FPSO-DAS system in real time so as to provide the operator ample time and information for the drift-off decision making.

In view of the the limitations of the aforementioned works, the contribution of this study are as follows:

- The operational safety limits of the DP FPSO in the production phase are evaluated and predicted in real time.
- The dynamic responses of DP FPSO, flexible jumper, artificial seabed, rigid riser, taut tether and the interconnected relationships among them are taken into consideration globally.
- The surrogate model is established to reduce the computational cost due to frequent numerical simulation so as to provide the operator ample time and information for the drift-off decision making.
- The statistical model is established to address the uncertainty due to randomness of sea states.

1.3. Structure of paper

The rest of paper is organized as follows. Section 2 presents the procedures and associated functions of the new probabilistic modelling methodology. Section 3 presents the case study of the FPSO and DAS coupling system to describe the application process and validate the accuracy of the proposed methodology. Section 4 presents the statistical distributions of the operational safety limits for the dynamic positioning of the FPSO, and compares the statistical performance of different operational safety limits.

2. Methodology

A 3-phase probabilistic modelling methodology, integrating the mechanical and surrogate models with the probabilistic model, is developed to predict the operational safety limits of the DP FPSO in concert with the DAS system, as illustrated in Fig.2. The mechanical model is a time domain simulation of the FPSO and DAS coupling system, which is used to evaluate the integrity of the FPSO and DAS coupling system and determine the operational safety limits of the FPSO. However, the computational cost could be too massive due to the large number of statistical samples generated for varying environmental conditions. In order to overcome this limitation, the surrogate model is established as an alternative to generate large samples, which is on the basis of small amount samples obtained from the mechanical model and thus reduce the computational cost. The probabilistic model is built to generate the sample set and simulate the statistical distribution of the operational safety limits, on the basis

of the MC simulation. In this simulation, the input is the statistical property of environmental conditions while the output is the statistical distribution of the operational safety limits for the dynamic positioning of the FPSO.

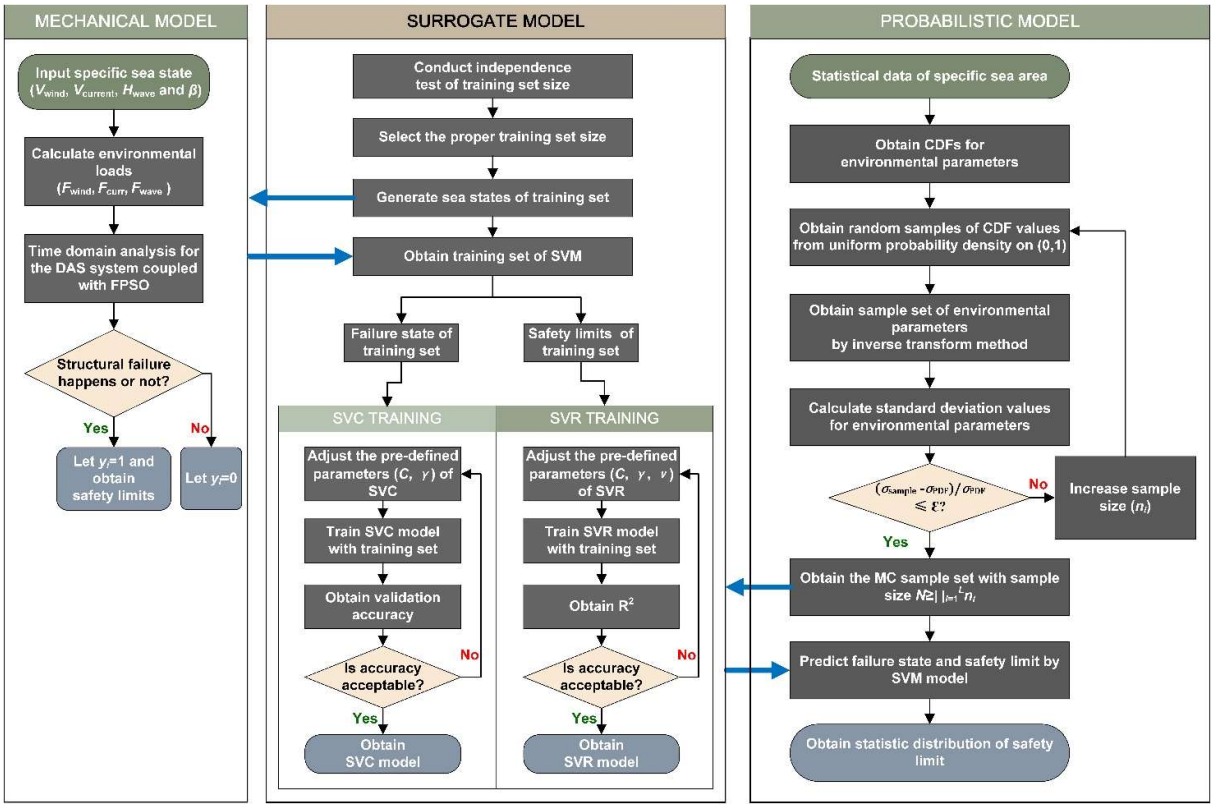

Fig. 2. Flowchart of the 3-phase probabilistic modelling methodology.

2.1. Mechanical model

2.1.1. Governing equations

The time domain analysis of the fully coupled FPSO-DAS system is conducted to determine the operational safety limits for a given environmental load condition. Notably the following governing equations for different structures are based on the respective body-fixed coordinate systems. It is assumed that FPSO is rigid and undergo six independent degrees of motion——three translational and three rotational. The governing equation of the FPSO's motion is written as follows:

$$m\ddot{x}_{\mathrm{buo},i} + C_i\dot{x}_{\mathrm{buo},i} + R_i x_{\mathrm{buo},i} + F_{\mathrm{jum}} + F_{\mathrm{buo}} = F_{\mathrm{wind}} + F_{\mathrm{curr}} + F_{\mathrm{wave}} + F_{DP} \quad (1)$$

where the subscript i=1,2,3,4,5,6 refers to the component of six degrees of freedom motion respectively; x is the translational or rotational motion along different axes; m is the mass of FPSO; C is the damping term; R is the righting moment of FPSO; F_{jum} is the response force of the flexible jumper; F_{buo} is the buoyance of FPSO; F_{wind}, F_{curr} and F_{wave} are the environmental loads caused by wind, current and wave respectively; F_{DP} is the response force of the DP system which is set to be 0 as the DP system fails to work in the drift-off scenario.

Flexible jumper bridges between the FPSO internal turret and gooseneck assembly on artificial seabed. The

flexibility of flexible jumper, such as elongation and bending, is revealed by the multi-layered structure consisting of metallic and polymer layers. Therein, multiple layers play different roles in maintaining a sufficient stiffness for tension and preventing excessive bending stress. In this paper, the mechanical model of flexible jumper is simplified as a single line model with the equivalent properties of multi-layered structure obtained from existing test data. The governing equation of the flexible jumper is written as:

$$EI\frac{\partial^2\alpha}{\partial s^2}\sec\alpha + (w - f_{\text{buo}})s - \int_0^s \left(f_{\text{env,n}}\sec\alpha + \sec^2\alpha\left(\frac{d\alpha}{ds}\right)\int_0^\xi \left(f_{\text{env,n}}\sin\alpha - f_{\text{env,t}}\cos\alpha\right)d\xi\right)ds = F_{\text{eff}}\tan\alpha - Q \tag{2}$$

where EI is the equivalent bending stiffness; α is the angle with respect to the horizontal line along the flexible jumper; ds and $d\xi$ are the differential elements of the arch-length of the flexible jumper ranging from 0 to the total length l; f_{buo} is the buoyance of flexible jumper; f_{env} is the environmental force according to the Morison equation; the subscript n and t refer to the normal and tangential components respectively; w is the wet weight per unit length; F_{eff} and Q are the effective tension and shear force respectively.

Let $\Delta\alpha$, ΔF_{eff} and ΔQ be the small perturbations of the variables: α, F_{eff} and Q, respectively. The total response of the flexible jumper is expressed by:

$$\begin{cases}\alpha_{\text{total}} = \alpha + \Delta\alpha \\ F_{\text{eff,total}} = F_{\text{eff}} + \Delta F_{\text{eff}} \\ Q_{\text{total}} = Q + \Delta Q\end{cases} \tag{3}$$

The dynamic equilibrium equation can be derived by substituting Eq. (3) into Eq. (2):

$$\begin{cases}\frac{\partial F_{\text{eff,total}}}{\partial s} - \left(F_{\text{eff,total}}\Delta\alpha + Q_{\text{total}}\right)\frac{d\alpha}{ds} - \frac{\partial}{\partial s}\left(Q_{\text{total}}\Delta\alpha\right) + f_{\text{env,t}} = (w - f_{\text{buo}})\frac{\partial^2 u_t}{\partial t^2} \\ \frac{\partial Q_{\text{total}}}{\partial s} - \left(F_{\text{eff,total}} - Q_{\text{total}}\Delta\alpha\right)\frac{d\alpha}{ds} + \frac{\partial}{\partial s}(T\Delta\alpha) + f_{\text{env,n}} = (w - f_{\text{buo}})\frac{\partial^2 u_n}{\partial t^2}\end{cases} \tag{4}$$

where u is the displacement caused by perturbations at s.

The effective tension of flexible jumper is expressed by:

$$F_{\text{eff}} = T + A_{\text{o}}p_{\text{o}} - A_{\text{i}}p_{\text{i}} \tag{5}$$

$$T = E(A_{\text{o}} - A_{\text{i}})\varepsilon \tag{6}$$

where T is the actual tension of the flexible jumper; A_{o} and A_{i} are the external and internal cross-sectional areas of the flexible jumper respectively; p_{o} and p_{i} are the corresponding fluid pressures respectively; ε is the strain of the flexible jumper.

In addition, the bend radius (χ) along the flexible jumper is calculated by:

$$\chi = \left(\frac{d\alpha}{ds}\right)^{-1} \tag{7}$$

The maximum allowable value of F_{eff} and minimum allowable value of χ are utilized as critical parameters to evaluate the safety integrity of the DAS system.

Different from flexible jumper, the deformation of rigid riser is only allowed in a smaller range, which means only bending is taken into consideration in the model. The governing equation of the rigid riser is written as:

$$\frac{\partial^2}{\partial z^2}\left[EI\frac{\partial^2 \delta}{\partial z^2}\right] - F_{\text{eff}}\frac{\partial^2 \delta}{\partial z^2} - q\frac{\partial \delta}{\partial z} + w\frac{\partial^2 \delta}{\partial t^2} = f_{\text{env}} \tag{8}$$

$$\varepsilon = \sigma / E_{\text{eff}} \qquad 4 \tag{9}$$

where δ is the deflection along the rigid riser; ε and σ are the strain and stress along the rigid riser respectively; E_{eff} is the effective Young's modulus. The boundary conditions of the rigid riser and taut tether at the bottom side are given by $\delta = 0$. The maximum allowable value of the compression strain and effective stress are also utilized as critical parameters to evaluate the safety integrity of the DAS system.

2.1.2. Environmental loads

It is assumed that wind and current are independent of time. The wind, current, and wave loads on FPSO can be calculated by:

$$F_{\text{wind}} = \frac{1}{2} C_{\text{wind},i} \rho_{\text{air}} V_{\text{wind}}^2 A_{\text{wind},i} \tag{10}$$

$$F_{current} = \frac{1}{2} C_{current,i} \rho_{sea} V_{current}^2 A_{current,i} \tag{11}$$

$$\begin{cases} F_{\text{wave},1st} = \int S(\omega)\text{RAO}(\omega, \beta, i)d\omega \\ F_{\text{wave},2nd} = \int S(\omega)\text{QTF}(\omega, \beta, i)d\omega \end{cases} \tag{12}$$

where $C_{\text{wind},i}$ is the wind drag coefficient for the different motion degree i; $C_{\text{current},i}$ is the current drag coefficient for the different motion degree i; ρ_{air} is the air density; V_{wind} is the magnitude of the relative velocity of the air past FPSO and A_{wind} is the projected area of FPSO above the water surface; V_{current} is the current velocity at the water surface, and assumed to be constant with the FPSO's draft; $S(\omega)$ is the wave spectrum; ω is the angular frequency of wave; RAO and QTF are the response amplitude operator and quadratic transfer function respectively; β is the incident wave direction.

2.2. Probabilistic model

It can be envisaged that there are significant variations in the magnitude and direction of environmental loads. In general, wind, current and wave loads are random and the correlative parameters which could be described by specific statistical properties. It is recognized that the operational safety limits will also be characterized with statistical properties.

Three different Weibull distribution are adopted to express the statistical properties of the mean wind speed (V_{wind}), surface current speed (V_{current}), and maximum wave height (H_{max}) respectively [20-22]. The corresponding cumulative distribution functions (CDFs) of V_{wind}, V_{current}, and H_{max} are expressed by:

$$CDF(V_{\text{wind}}) = 1 - exp[-\left(\frac{V_{\text{wind}}}{c_{\text{wind}}}\right)^{k_{\text{wind}}}] \tag{13}$$

$$CDF(V_{\text{current}}) = 1 - exp[-\left(\frac{V_{\text{current}}}{c_{\text{current}}}\right)^{k_{\text{current}}}] \tag{14}$$

$$CDF(H_{\text{max}}) = 1 - exp[-\left(\frac{H_{\text{max}} - H_0}{H_c - H_0}\right)^{k_{\text{wave}}}] \tag{15}$$

where c_{wind} (c_{current}, H_c) and k_{wind} (k_{current}, k_{wave}) are the scale parameter and shape parameter of Weibull distribution

respectively; H_0 is the minimum threshold level for different sea areas.

The relationship between the significant wave height (H_{wave}) and H_{max} is given by [23]:

$$H_{\max} = kH_{\text{wave}} \tag{16}$$

where k is the scale parameter associated with the number of waves. Thus, H_{wave} and H_{max} follow the same Weibull distribution for the specific k.

The relations between H_{wave} and T_{wave} can be expressed by the power function as:

$$T_{\text{wave}} = b_{\text{T}} H_{\text{wave}}^{k_T} \tag{17}$$

where b_T and k_T are the scale and shape parameter respectively, which are deterministic for the specific sea area.

Therefore, the operational safety limit (expressed by the polar coordinates as R and θ) is the function of V_{wind}, $V_{current}$, and H_{wave} for the DAS system. On the basis of the MC simulation, the unknown CDF of the operational safety limit can be expressed by:

$$CDF_{\text{u}}(R,\theta) = \iint \frac{1}{N}\sum_{j=1}^{N} \delta(R - R_j)\delta(\theta - \theta_j)\, dRd\theta \tag{18}$$

where δ(x) is the Dirac delta function. When the sample size N approaches infinity, the CDF_u will equal to the actual CDF:

$$\lim_{N\to\infty} \overline{CDF}(R,\theta) = CDF(R,\theta) \tag{19}$$

Eq. (19) indicates that N should be large enough to control the error.

It is assumed that CDFs are random variables with uniform probability density on (0, 1). Based on the inverse transform method, the values of V_{wind}, $V_{current}$ and H_{wave} can be obtained by:

$$x = CDF^{-1}(u) \tag{20}$$

where x refers to V_{wind}, $V_{current}$ or H_{wave}; u is a random number sampling from (0, 1).

It is assumed that V_{wind}, $V_{current}$, H_{wave} and β are independent random variables for the MC simulation, and the sample size N should obey the following rule to make the sampling error acceptable:

$$N \geq \prod_{l=1}^{L} n_l^L \tag{21}$$

where n_l is the least sample size satisfying the precision for a single variable and L is the number of random variables.

2.3. Surrogate model

As aforementioned, the surrogate model is required to cut down the computational cost due to the frequent numerical simulations for the large sample set obtained from the probabilistic model. The methods for surrogate models can be further divided into supervised and unsupervised [24]. The unsupervised method performs prediction with less manual interference and training labels. However, large training set is required for unsupervised method [25], which is contrary to the aims of introducing surrogate model. Among the supervised methods, artificial neural network (ANN) and support vector machine (SVM) are prior to others because these two methods possess higher precision and efficiency with the same training set [26]. Moreover, SVM can gain higher precision with smaller

training set than normal ANN. Although the advanced deep learning techniques are proposed to enhance the precision of ANN, the limitation of large training set is still unsolved. Thus, SVM is applied in this paper as the surrogate model.

A large sample size is required to cover the sample of the extreme sea state, the occurrence rate of which is less than 10^{-5} [20]. Nonetheless, the calculation of large sample set results in huge computational cost. In view of this, the surrogate model is established on the basis of the support vector machine (SVM) algorithm. SVM is the state of the art of surrogate modeling techniques, and it shows a great advantage of reducing the computational expense for a complex model [27, 28].

Two different SVM models, i.e. support vector classification (SVC) and support vector regression (SVR) models are adopted in two phases. The SVC model plays the role of classifying the data by determining whether the structure failure of the FPSO and DAS coupling system happens or not in the specific duration, whereas the SVR model is utilized to predict the position of the operational safety limit.

SVC is utilized to perform the classification function by solving the optimization equation as:

$$\min_{w,\xi} \frac{1}{2} w^T w + C \sum_{i=1}^{L} \xi_i \tag{22}$$

$$\text{subject to } y_i(w^T \phi(x_i) + b) \geq 1 - \xi_i$$

$$\xi_i \geq 0, i = 1, \ldots, L.$$

The dual is

$$\min_{\alpha} \frac{1}{2} \alpha^T Q \alpha - e^{\mathrm{T}} \alpha \tag{23}$$

$$\text{subject to } y^T \alpha = 0,$$

$$C \geq \alpha_i \geq 0, i = 1, \ldots, L.$$

where w is a weight parameter; ξ is the slack variable; i represents the i_{th} sample from the training dataset whose size is L; $y_i \in \{0,1\}$ is the output label (0 and 1 referring to not failure and failure respectively) while $x_i \in R^N$ is the training vector; C is the cost parameter pre-defined for adjusting the optimization step size; Q is an L-order matrix, and $Q_{ij} = y_i y_j K(x_i, x_j)$; α_i is the Lagrange multiplier. Radial basis function (RBF) is set as the kernel function $K(x_i, x_j)$:

$$K(x_i, x_j) = \exp(-\gamma_{\text{RBF}} ||x_i - x_j||^2) \tag{24}$$

where $-\gamma_{\text{RBF}}$ is also the pre-defined parameter for controlling the optimization progress. The final decision function is given by solving Eq. (23) as:

$$\hat{y} = sgn(\sum_{i=1}^{L} y_i \alpha_i K(x_i, x_j) + b) \tag{25}$$

SVR is utilized to predict the operational safety limits, with the optimization equations given by:

$$\min_{w,b,\xi,\xi^*,\epsilon} \frac{1}{2} w^T w + C[\nu\epsilon + \frac{1}{l}\sum_{i=1}^{L}(\xi_i + \xi_i^*)] \tag{26}$$

$$\text{subject to } (w^T \phi(x_i) + b) - z_i \leq \epsilon + \xi_i,$$

$$\xi_i, \xi_i^* \geq 0, i = 1, \ldots, L, \epsilon \geq 0.$$

The dual is

$$\min_{\alpha,\alpha^*} \frac{1}{2}(\alpha - \alpha^*)^T Q(\alpha - \alpha^*) + z^T(\alpha - \alpha^*) \tag{27}$$

$$\text{subject to } e^T(\alpha - \alpha^*) = 0, e^T(\alpha + \alpha^*) \leq Cv,$$

$$C/L \geq \alpha_i, \alpha_i^* \geq 0, i = 1, \ldots, L.$$

where RBF is set as the kernel function of Eq. (27). The final decision function is given as:

$$\hat{y} = \sum_{i=1}^{L}(-\alpha_i + \alpha_i^*)K(x_i, x_j) + b \tag{28}$$

2.4. Implementation of three models

Three interconnected models are established sequentially on the basis of the aforementioned equations. It is noted that the output of systematic methodology is the statistic distribution of operational safety limits, and the input is the specific DAS system coupled with FPSO and the corresponding statistical parameters of sea area. The mechanical model is first established based on the specific DAS system as Eq. (1) ~ (12). Then the input environmental loads for the mechanical model is provided by a specific training set aiming to establish the surrogate model. The outputs of the mechanical model are the failure states and operational safety limits in relation to the environmental loads of this training set. The surrogate model is trained by this training set, and SVC and SVR models are established as Eq. (22) ~ (28). If the precisions of SVC and SVR models are acceptable, the surrogate model will be utilized to predict the failure states and operational safety limits for statistical analysis. On the other hand, the statistical parameters of sea area are utilized to establish the Weibull distributions respectively based on Eq. (13) ~ (15). Then the random sample sets of environmental loads are generated by inverse transform method as Eq. (20), which is the input of the surrogate model for the prediction of operational safety limits and failure states.

Specific procedures explained by the following algorithms are applied to obtain the specific outputs respectively. Algorithm_MEC presents the procedures of the determination of safety limits from the mechanical model, which is utilized to obtain the safety limit from the input data of sea states.

Algorithm_MEC. Determination of safety limits from mechanical model

Input:

- V_{wind}: the magnitude of the relative velocity of the air past FPSO.
- V_{current}: the current velocity at the water surface.
- H_{max}: the maximum wave height.
- β: the incident wave direction.

Output:

- Failure states (y_i) and operational safety limits.

Procedures:

1 Calculate environmental loads with input parameters;

2 Conduct time domain analysis for the established mechanical model with the environmental loads;
3 **if** the structure failure happens in the established mechanical model:
4 **if** {y_i=1; Obtain different operational safety limits;}
5 **else:** y_i=0;

Algorithm_MEC can be utilized to obtain the required operational safety limits for Algorithm_SUR which illustrates the procedures of the establishment of SVC and SVR models.

Algorithm_SUR. Establishment of surrogate models: SVC and SVR

Input:

- Training set size.
- Failure states (y_i) and operational safety limits based on the sea states from training set.
- Cost parameter set (***C***), kernel parameter set ($\boldsymbol{\gamma}$), Regression parameter set ($\boldsymbol{\nu}$)

Output:

- SVC model for the prediction of failure states.
- SVR model for the prediction of operational safety limits.

Procedures:

1 Conduct independence test: several training sets with different sizes are utilized to train the SVC and SVR models;
2 Obtain the training set with the most applicable size;
3 Utilize **Algorithm_MEC** to determine the failure states and operational safety limits for the training set;
4 **for** every C_i, γ_i in ***C***, $\boldsymbol{\gamma}$**do**
5 **if** Train SVC model;
6 **if** Obtain validation accuracy;
7 **if if** the validation accuracy is acceptable and optimal:
8 **if if** Obtain the specific SVC model with relative C_i and γ_i;
9 **for** every C_i, γ_i and v_i in ***C***, $\boldsymbol{\gamma}$ and $\boldsymbol{\nu}$ **do**
10 **if** Train SVR model;
11 **if** Obtain validation accuracy;
12 **if if** the validation accuracy is acceptable and optimal:
13 **if if** Obtain the specific SVR model with relative C_i, γ_i and v_i;

It is noted that lines 4 to 8 are the procedures of establishing SVC model, and lines 9 to 13 are the procedures of establishing SVR model. The SVC and SVR models output from Algorithm_SUR will be utilized as the surrogate models for Algorithm_PRO which presents the procedures of statistical analysis of safety limits for the specific sea area.

Algorithm_PRO. Statistical analysis of safety limits for specific sea area

Input:

- Statistical parameters of specific sea area: scale parameters (c_{wind}, c_{current} and H_c) and shape parameters (k_{wind}, k_{current} and k_{wave}).
- SVC model for the prediction of failure states.
- SVR model for the prediction of operational safety limits.
- Acceptable error index ε.

Output:

- Statistical distribution of operational safety limits.

Procedures:

Obtain $CDF(V_{wind})$, $CDF(V_{current})$, $CDF(H_{max})$ with scale parameters and shape parameters;
for every sample size n_i in $\boldsymbol{N}$ **do**
if Obtain random sample set $\boldsymbol{X}$ from uniform probability density on (0,1);
foCalculate inverse function values (V_{wind}, $V_{current}$, H_{max}) from $\boldsymbol{X}$ based on $CDF(V_{wind})$, $CDF(V_{current})$, $CDF(H_{max})$;
foCalculate standard deviation values ($\sigma_{sample,wind}$, $\sigma_{sample,\ current}$, $\sigma_{sample,\ wave}$) of environmental parameter sets ($\boldsymbol{V_{wind}}$, $\boldsymbol{V_{current}}$, $\boldsymbol{H_{max}}$);
foObtain $PDF(V_{wind})$, $PDF(V_{current})$, $PDF(H_{max})$ from $CDF(V_{wind})$, $CDF(V_{current})$, $CDF(H_{max})$;
foCalculate standard deviation values ($\sigma_{PDF,wind}$, $\sigma_{PDF,\ current}$, $\sigma_{PDF,\ wave}$) of $PDF(V_{wind})$, $PDF(V_{current})$, $PDF(H_{max})$;
if if $|\sigma_{sample,wind}-\sigma_{PDF,wind}|/\sigma_{PDF,wind}\leq\varepsilon$:
if if if $|\sigma_{sample,current}-\sigma_{PDF,current}|/\sigma_{PDF,current}\leq\varepsilon$:
if if ifif $|\sigma_{sample,wave}-\sigma_{PDF,wave}|/\sigma_{PDF,wave}\leq\varepsilon$:
if if ifif Obtain MC sample sets;
Predict failure states and operational safety limits of MC sample sets by SVC model and SVR model;
Obtain statistical distribution of operational safety limits;

3. Case study

3.1. Drift-off analysis to establish operational safety limits

3.1.1. Principle of operational safety limit determination

The operational safety limits are classified as three level: physical limit, red limit and yellow limit. The related definitions and the subsequent operational plans are described as follows.

- Physical limit: the safety integrity of one or more components of DAS system exceeds the allowable value.

  Operational plan: emergency quick disconnection (EQD) should be completed and the DAS system is disconnected to FPSO.

- Red limit: the safety integrity of one or more components of DAS system is about to exceed the allowable value within the critical required time of emergency disconnection sequence (EDS).

  Operational plan: EDS operations should be activated to ensure the success of EQD.

- Yellow limit: FPSO is about to reach the red limit within the preparation time of EDS.

  Operational plan: preparations for EDS operations should be initiated.

The principle of the operational safety limit determination for a given environmental condition is illustrated in Fig. 3(a). It can be seen from Fig. 3(a) that the physical limit is determined first, on the basis of the safety integrity of DAS system. The red limit and yellow limit are determined subsequently through a backward deduction of FPSO's displacement based on the time required for EDS and its preparation respectively. The time required for

EDS and its preparation is related to operating rules and operators, and should be determined separately. Based on the industry standard and guideline, it is recommended to set the time for EDS and its preparation as 40s and 45s respectively [29, 30]. Besides, in view of the potential structural damage of the FPSO and DAS coupling system, four critical parameters i.e. the maximum effective tension (MET), minimum bend radius (MBR), maximum effective stress (MES) and maximum compression strain (MCS) are identified to evaluate the safety integrity of the DAS system, as tabulated in Table 1. The MET and MBR are critical parameters to determine whether a structural failure occurs to the flexible jumper, while the MES and MCS are critical parameters for the rigid riser. The coordinate system used to describe the operational safety limit position and environmental load direction are defined in Fig. 3(b).

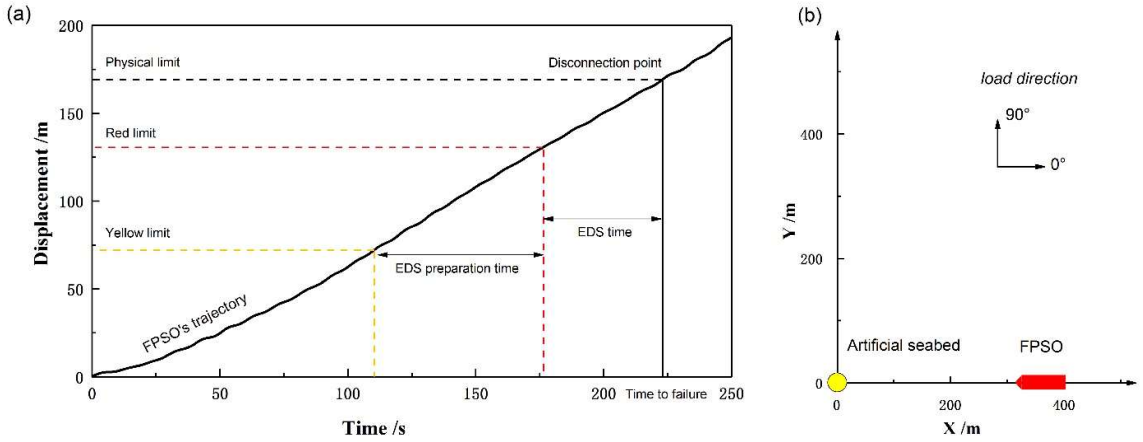

Fig. 3. (a) Principle of safety limit determination; (b) Coordinate system.

Table 1. Critical parameters of the DAS system.

Parameter	Allowable value	Reference
MBR	3.3495 m	Handbook on design and operation of flexible pipes (2017)
MET	4435 kN	
MES	348 MPa	API RP 2RD
MCS	2.16%	DNV-OS-F101

3.1.2. Operational safety limit determination

The mechanical model of the FPSO and DAS coupling system is established to determine the operational safety limit, and the time domain analysis is conducted by the finite element program. The key design parameters of the FPSO and DAS coupling system, which have been verified to satisfy the design requirement in the aspects of strength, buckling, stability, etc. [4, 31, 32], are tabulated in Table 2. The parameters associated with environmental loads in 1-year, 10-year, and 100-year sea states are tabulated in Table 3 respectively.

Table 2. Key design parameters of the system.

FPSO		Flexible jumper		Rigid riser	
Length, *L* (m)	224	Horizontal span, *s* (m)	366	Length, *h* (m)	2797.5

Board, B (m)	41.5	Submerged depth, d (m)	200	Outer diameter (CP), D_c (m)	0.3239
Depth, D (m)	24	Length, l (m)	696	Weight per unit, w (kN/m)	1.999
Draught, d (m)	16	Weight per unit, w (kN/m)	0.186	Top tension factors	1.7
Centre of gravity, H_g (m)	13.5	Outer diameter, D_o (m)	0.276	Bend stiffness, EI_t (kN·m^2)	4.62×10^4
Capacity, Δ (tons)	125700	Inner diameter, D_i (m)	0.203	Axial stiffness, EA_t (kN)	3.78×10^6
		Bend stiffness, EI_j (kN·m^2)	34.2	Water depth, H (m)	3000
		Axial stiffness, EA_j (kN)	3.27×10^4		

Table 3. Environmental parameters associated with different sea states.

	1-year-condition	10-year-condition	100-year-condition
Wind velocity, V_{wind} (m/s)	16.40	18.60	39.00
Wave height, H_{wave} (m)	13.24	15.72	17.35
Wave period, T_{wave} (s)	13.11	14.20	14.87
Current velocity, $V_{current}$ (m/s)	1.22	1.38	1.78
Load direction, β (°)		0; 180	

Fig. 4 illustrates the time histories of the critical parameters for the 1-year environmental condition with the load directions of 0° and 180° respectively. It can be seen from Fig. 4 that the MBR and MET of the flexible jumper increase over time, whereas the MES and MCS of the rigid riser are nearly constant. This reflects the decoupled effect of the flexible jumper can isolate the response of the DAS system from the FPSO's motion effectively, which is in consistent with the existed research [6].

It is shown in Fig. 4 that the structure integrity of the flexible jumper dominates the physical limit determination. For the load direction 0°, MBR of flexible jumper reaches the allowable value first when the drift-off time is 364.3 s. Therefore, EDS should be completed before this time. The corresponding time to failure is 322.9 s for the load direction 180°, which is also determined by the MBR failure. The physical limits for the two cases are illustrated in Fig. 5. It is noteworthy that, for the load direction 0°, the MBR failure, which occurs at the joint-point between the bend stiffener and flexible jumper, is caused by the over-pulling of the flexible jumper. On the contrary, for the load direction 180°, the MBR failure occurs at the overhanging point of the flexible jumper due to the over-bending of the flexible jumper. For this reason, the physical limit of FPSO, with respect to the load direction 0°, is located at the far end, but when FPSO is subject to 180-degree environmental loads, the physical limit is located at the near end.

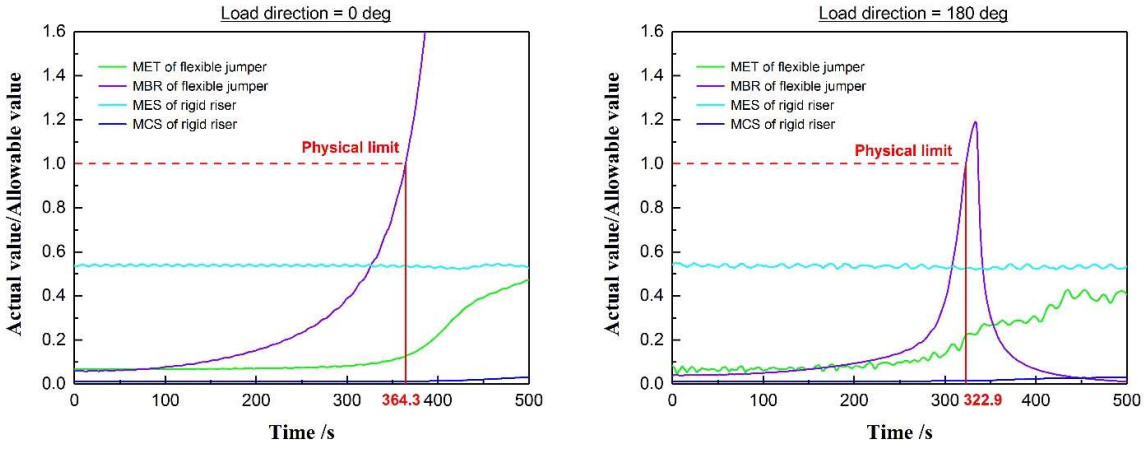

Fig. 4. Time history of critical parameters (1-year-condition).

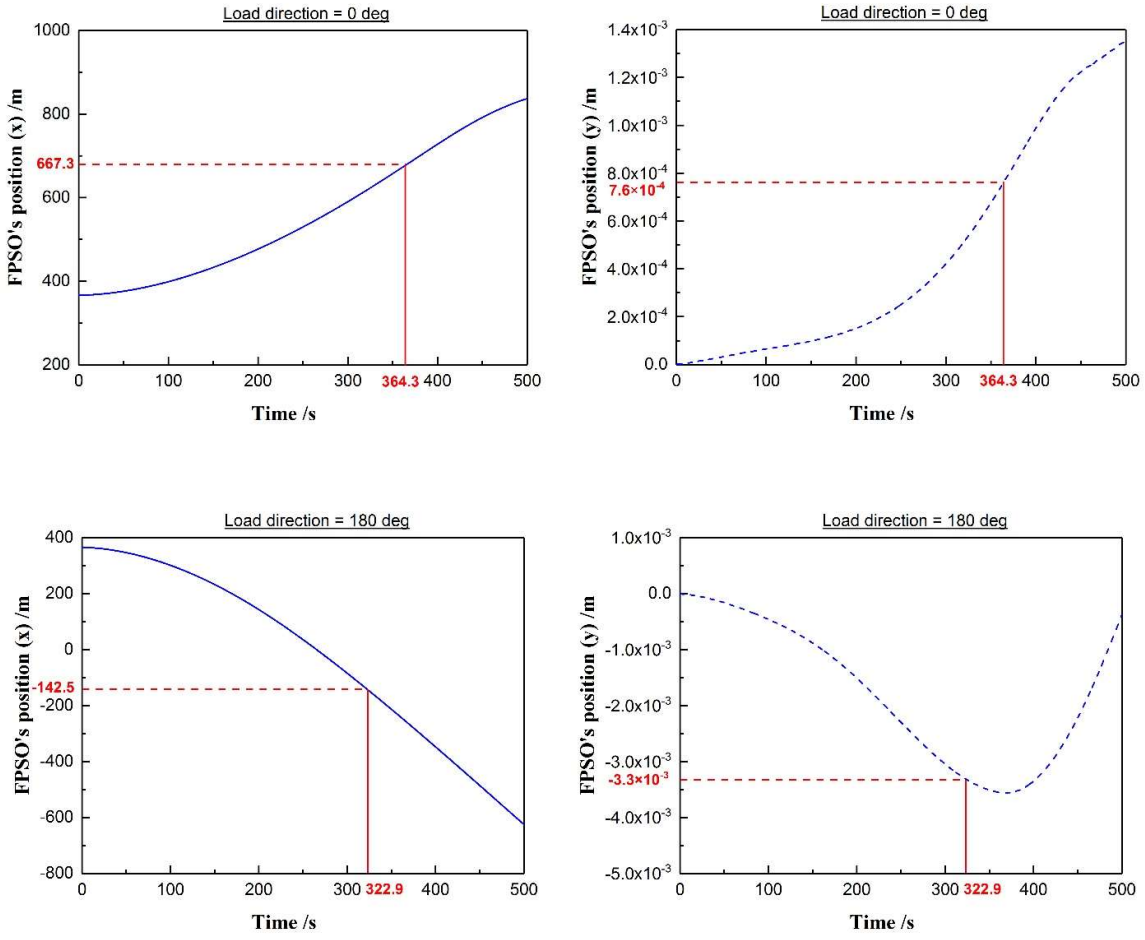

Fig. 5. Position of physical limit (1-year-condition).

3.1.3. Sensitivity analysis

In order to investigate the influences of environmental loads on each operational safety limit and determine the

relevance between associated parameters and safety limits, an importance analysis for parameters is conducted. Fig. 6 depicts the rate-of-change of these parameters on the positions of each operational safety limit, in a polar coordinate system (where R and θ refer to radius and angle coordinates respectively). It can be seen from Fig. 6 that the direction of environmental loads dominates the variation in the angle coordinate of the safety limit. The wave height and current velocity have limited effect on the physical limit for the reason that the physical limit is mainly determined by the structure integrity of the flexible jumper. However, the wave height and current velocity have significant influences on red and yellow limits due to their contribution to the time to failure. It can also be seen from Fig. 6 that the wind velocity has insignificant effect on each operational safety limit, in comparison with other parameters. Therefore, the wind velocity can be ignored when establishing the surrogate model, because irrelevant input parameters in the training set will lead to disturbance for prediction.

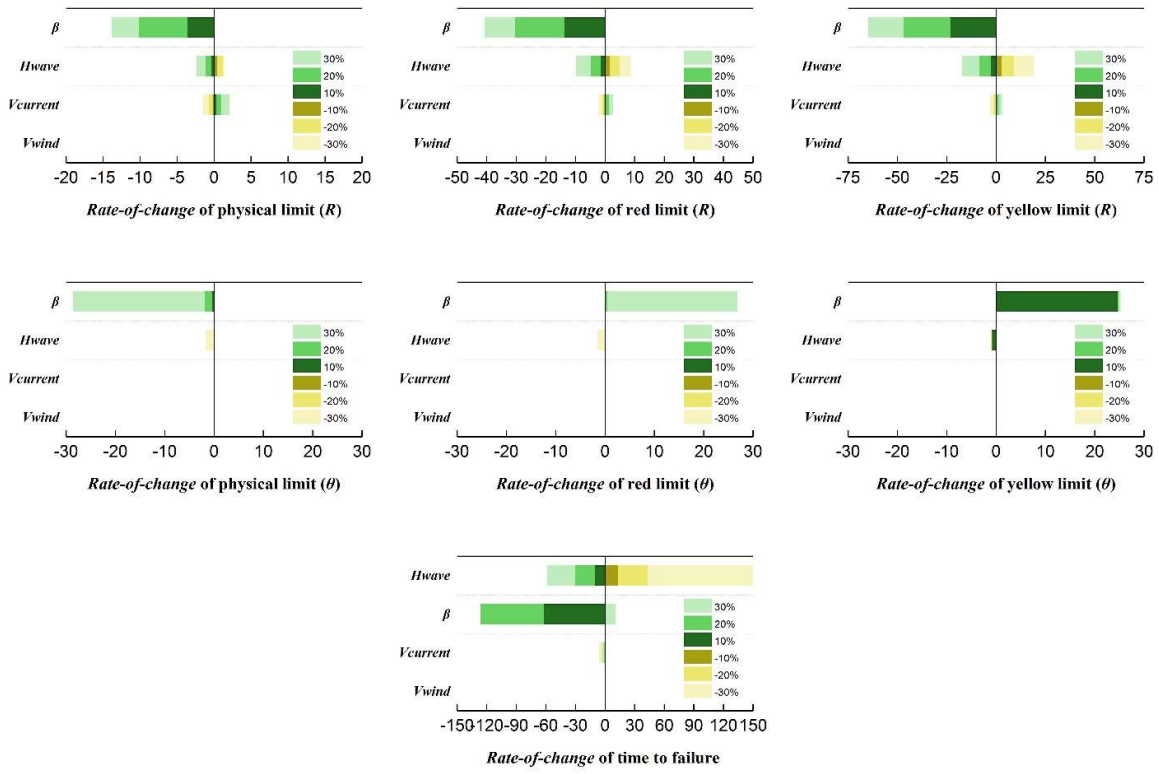

Fig. 6. The relative importance of parameters on the operational safety limits and time to failure.

3.2. Statistical properties of environmental loads

The statistical properties of environmental loads for a specific sea area in South China Sea are listed in Table 4. It is assumed that the probability density function (PDF) of β is the uniform probability density on (0, 180). To meet the accuracy requirement, the 1,000,000 samples of environmental loads are generated randomly in accordance with Eq. (20).

Table 4 Statistical properties of V_{current} and H_{wave} (see definition of parameters in Eq. 14-16)

Item	Parameter	$V_{current}$	H_{wave}
Shape parameter	$k_{current}$, k_{wave}	0.01	1.20
Scale parameter	$c_{current}$, H_c	0.6	1.84
Threshold level	H_0	-	0.08

3.3. Prediction of operational safety limits

3.3.1. Establishment of SVM

Based on the importance analysis of the parameters in Section 3.1.3, the wave height, current velocity and load direction are set as the inputs of the SVM model.

The SVM model consists of one SVC model and six SVR models for the classification of the failure states and the prediction of the operational safety limits respectively. The training set of the SVC model is predefined by dividing cases into two categories, i.e. failed and safe, with the output label assigned 1 and 0 respectively. The training set with output label 1 will be further utilized as the training set of the SVR models. Therefore, the output of the SVC model is the failure state, while the outputs of the SVR models are the positions of physical, red and yellow limits respectively.

Expansion of the training set will increase the accuracy of the SVM model, but accuracy will gradually converge to a stable level. Thus, the independence test of the training set size is conducted to determine a suitable size to ensure acceptable computational cost and fitting goodness as well. The validation accuracy of SVC and the minimum R^2 of SVR for three typical training sets are listed in Table 5 while these datasets are obtained from the numerical simulation. The Dataset 2 is selected as the training set based on the trade-off between the computational cost and fitting goodness.

Table 5 Characteristics of three training sets in independence test.

Item	Dataset 1	Dataset 2	Dataset 3
Case number for $V_{current}$	5	7	9
Case number for H_{wave}	5	7	9
Case number for β	7	9	11
Training set size	175	441	891
Validation accuracy (%)	97.14	99.54	100.00
Minimum R^2	0.9524	0.9997	0.9999

3.3.2. Validation of SVM

As aforementioned in Section 2.3, three parameters, i.e. C, γ_{RBF} and v, which can affect the precision of the SVM model to a large extent, should be pre-defined before training the SVM model. To avoid overfitting and underfitting, the suitable values for these parameters are searched from a specific interval, as listed in Table 6.

Table 6 Searching interval of user pre-defined parameters for SVM models.

Item	SVM model	Interval	Optimized result

Cost parameter C	SVC & SVR	$2^{-16} \sim 2^{16}$	2
Kernel parameter γ_{RBF}	SVC & SVR	$2^{-10} \sim 2^{10}$	32
Regression parameter v	SVR	0.00 ~ 0.99	0.50

The accuracy of the SVC model is verified by the comparison of the training label (y_i) and predicting label ($\hat{y}_i$), as depicted in Fig. 7. It can be seen from Fig. 7 that most of the samples in the predicting set are consistent with the training set, except for two samples marked with the specific color and size. Meanwhile, the regression fitness of SVR models are verified, as depicted in Fig. 8. It can be seen from Fig. 8 that the training result is in highly consistent with the testing result for every SVR model, with the value of R^2 larger than 0.9997. Therefore, the accuracy of the SVM model has been validated, and this model can be further adopted for the prediction of the operational safety limit position.

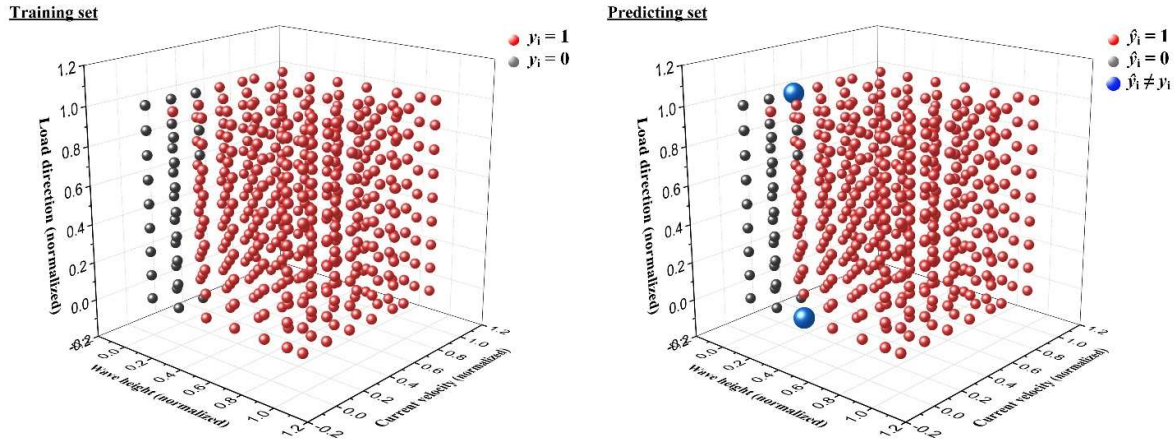

Fig.7. Validation of the accuracy for the SVC model.

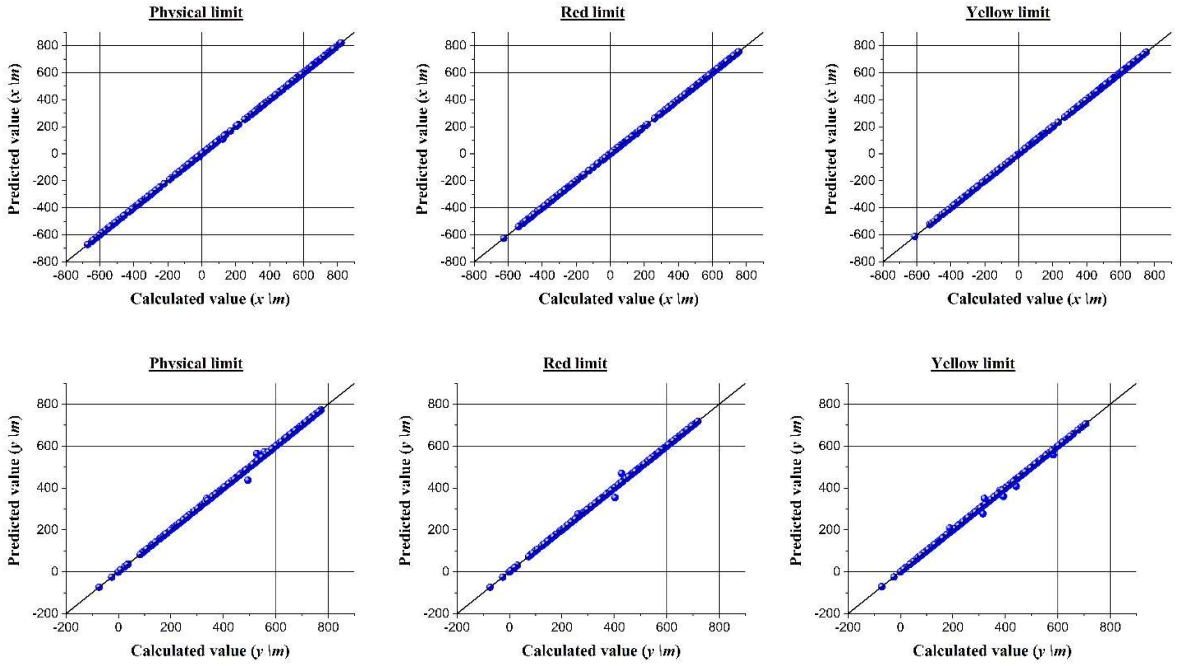

Fig.8. Validation of the accuracy for the SVR models.

4. Results and discussions

4.1. Statistical analysis of operational safety limit

On the basis of 1,000,000 samples of environmental loads, the predicted results of SVR models as different operational safety limits are obtained and summarized. The occurrence rates of 1,000,000 obtained results (physical limits, red limits and yellow limits) are depicted in Figs. 9~11 respectively and defined as the "frequency" of operational safety limits. These figures are the 3-d illustration of the statistical distribution of obtained operational safety limits. The area marked with dark red means the range of operational safety limits which possesses the highest frequency, while the area marked with dark blue means the range with lowest frequency.

It is noteworthy that eighteen percent of samples are safe cases where the structural failure did not occur throughout the drift-off process, due to the encountered wave and current with the slight amplitude. It is shown in Fig. 9 that more than 80% physical limits are concentrated within the radius between 600~750 meters, because physical limits are mainly determined by the safety integrity of the flexible jumper. This is in consistent with the results of the importance analysis and verifies the effectiveness of the proposed methodology. It can be seen from Fig. 10 and Fig. 11 that most of red and yellow limits are scattered within the radius between 600~700 meters, but the congregated area of the high-frequency points for yellow limits is smaller.

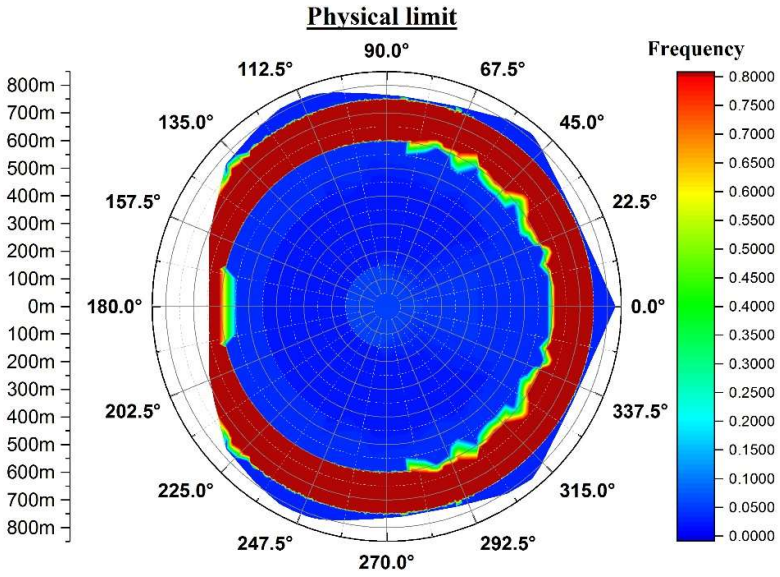

Fig. 9. Frequency contours of physical limits.

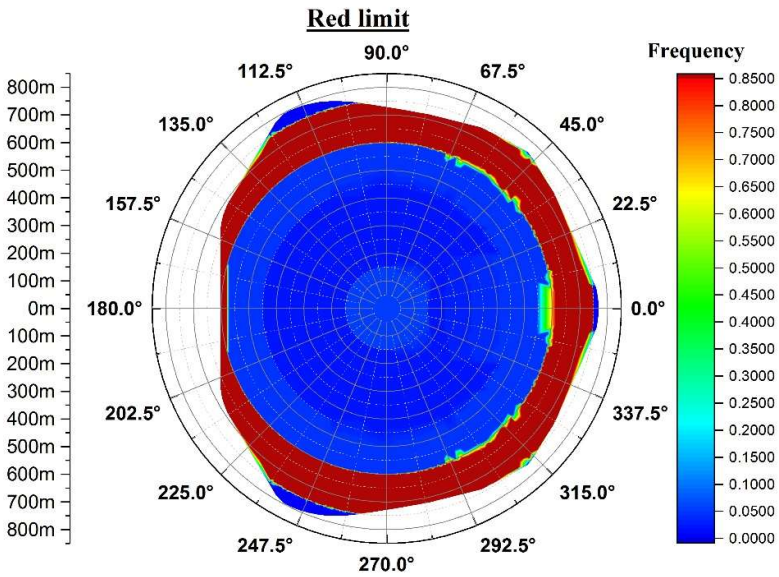

Fig. 10. Frequency contours of red limits.

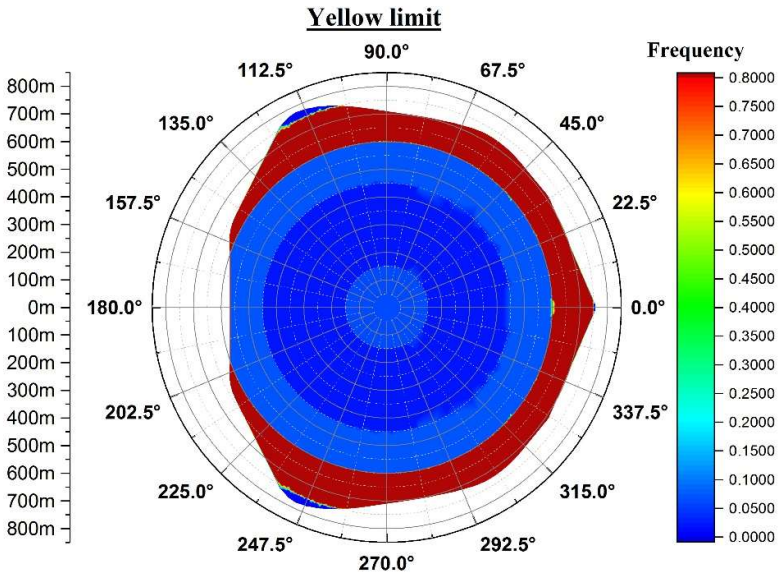

Fig. 11. Frequency contours of yellow limits.

Aiming at systematically investigating the distribution regularities of the operational safety limits, the angle range between 0 and 180 degrees is evenly divided into 8 intervals. The frequencies of the operational safety limits for different angle intervals are illustrated in Figs. 12~14 respectively. It can be seen from Fig. 12 that in the angle range between 22.5 and 157.5 degrees, a frequency peak occurs at around 700 meters, due to the MBR failure at the connection between the flexible jumper and bend stiffener. In the interval of 157.5~180 degrees, the frequency peak is at around 40 meters due to the MBR failure at the overhanging point of the flexible jumper. It is noteworthy that in the interval of 0~22.5 degrees, there are two frequency peaks occurring at around 720 and 30 meters,

corresponding to the different failure sites of the flexible jumper.

It can be seen from Fig. 13 that a frequency peak of red limit occurs at around 670 meters in the interval of 22.5~157.5 degrees, except for the range of 90~112.5 degrees where the frequency peak occurs at around 690 meters. On the other hand, another frequency peak in the interval of 0~22.5 degrees is located at around 70 meters. In the interval of 157.5~180 degrees, the frequency peak is located at around 40 meters. Likewise, it can also be seen from Fig. 14 that a frequency peak of yellow limit occurs at around 660 meters in the interval of 22.5~90 degrees. The frequency peak in the intervals of 90~112.5 degrees, 112.5~135 degrees, 135~157.5 degrees and 157.5~180 degrees are located at around 680 meters, 580 meters, 640 meters and 40 meters respectively. Partial results of red limit and yellow limit reveals stronger randomness than physical limit because of the difference between the initial FPSO orientation and direction of environmental loads.

It is noteworthy that most of the operational safety limits are located at the far end and near end relative to the artificial seabed, and the operational safety limits located within 0~90 degrees possess higher frequencies than that within 90~180 degrees, because of the impact of the second-order wave drift force on the FPSO motion amplitude. The drift force varies with the wave load direction due to the variation of the entrance section shape. In the oblique waves ranging from 0 to 90 degrees, the entrance section of wave is mainly located at the bow which is characterized with the prominent streamline shape, resulting in much smaller vertical drift force than horizontal component, and thus the sway motion of FPSO is negligible in comparison with the surge motion. For this reason, the FPSO drifts towards the far end relative to the artificial seabed, reaching to far-end safety limits. In the oblique waves ranging from 90 to 180 degrees, the streamline shape of stern is insignificant, resulting in the more sway motion of FPSO than the surge motion, and thus safety limits are located at the far end and within 0~90 degrees as well. However, when the wave load direction is 180 degrees, the surge motion dominates the drift of FPSO, and thus results in near-end safety limits.

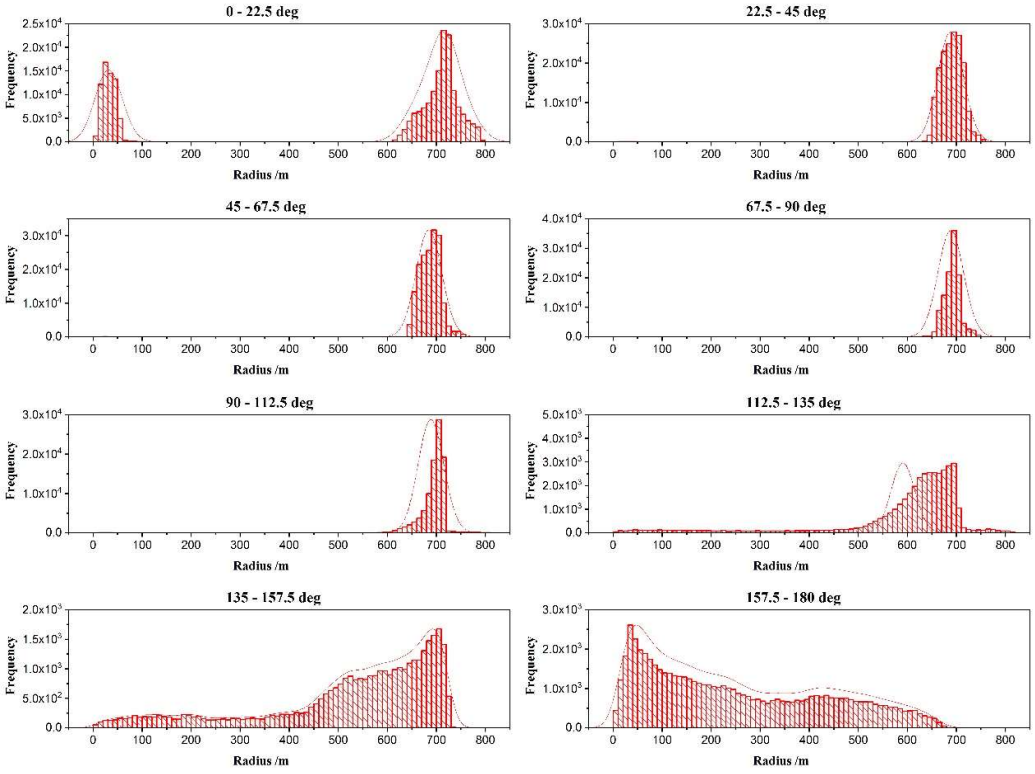

Fig. 12. Frequency of physical limit for different angle interval.

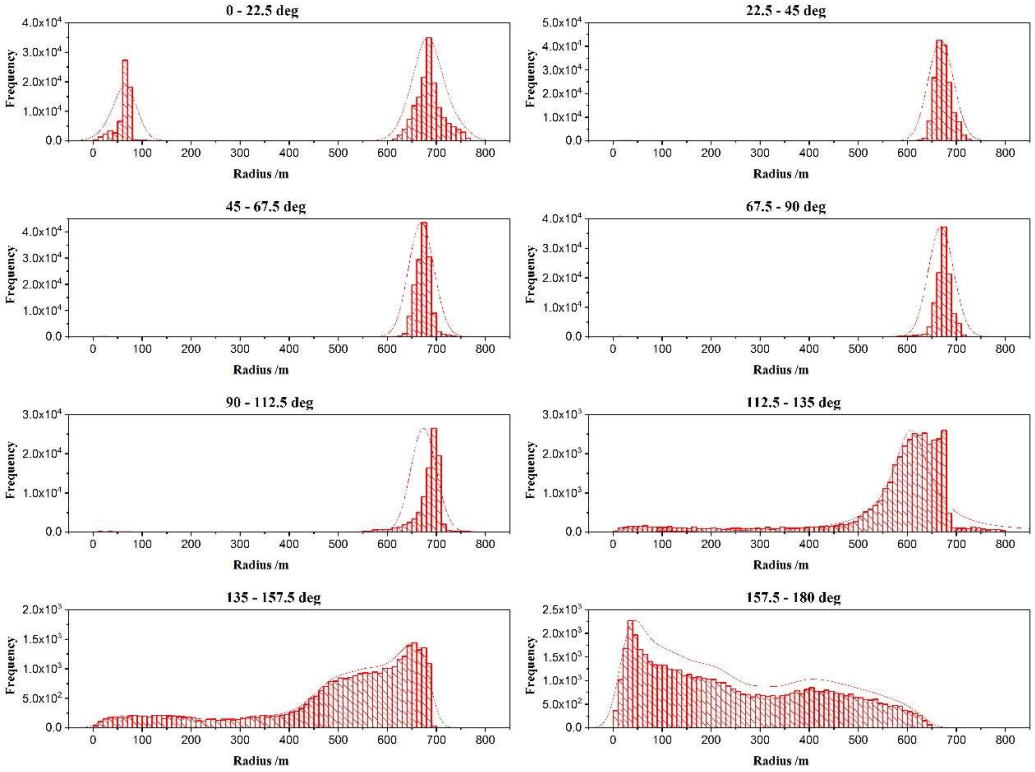

Fig. 13. Frequency of red limit for different angle interval.

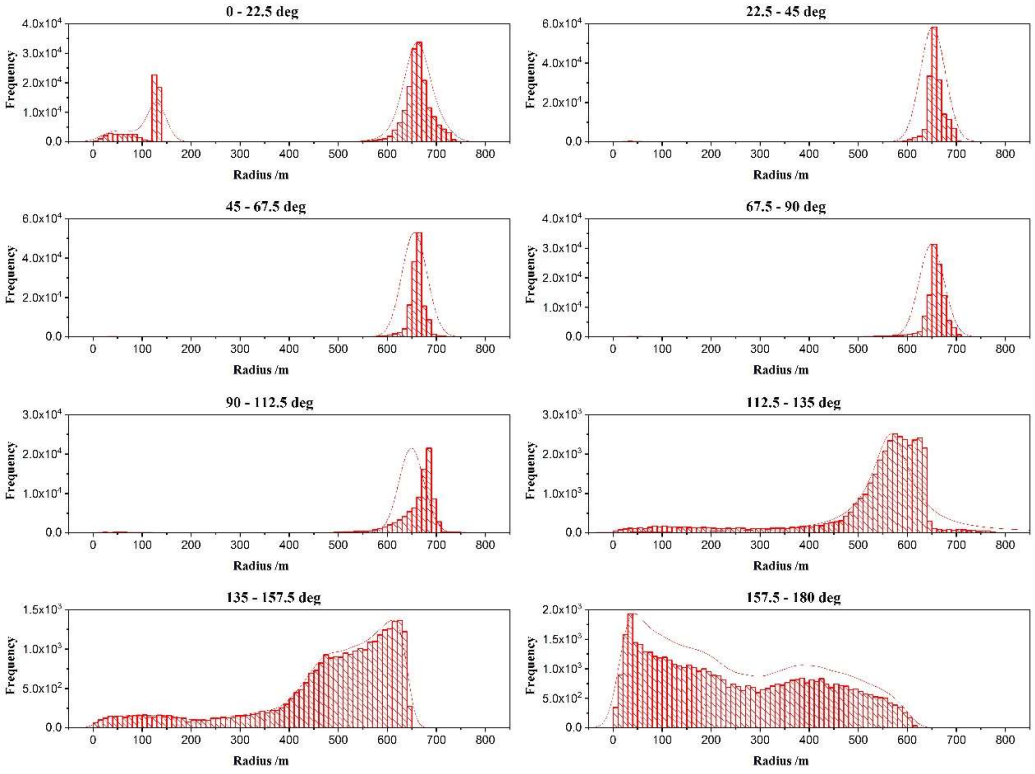

Fig. 14. Frequency of yellow limit for different angle interval.

4.2. Application of methodology to offshore sites

Environmental loads in different sea sites can influence the prediction of operational safety limit. The design information of the specific offshore site should be provided first before establishing the numerical mechanical model. Concurrently, the statistical data of the service sea area are collected to determine the probability distributions of environmental loads. Thereafter, the predictions of frequency contour of operational safety limit can be provided for warning signal and supporting decision makings.

Once the drift-off scenarios occurred on the offshore site due to the failure of DP system, the on-time location of FPSO should be provided to be compared with the frequency contour of operational safety limit, and the possibilities of FPSO breaking through different operational safety limits are obtained.

When FPSO breaks through the yellow limit with the highest possibility revealed in the frequency contour, preparations for EDS operations should be initiated. If FPSO continues to drift off and breaks through the red limit with the highest possibility, EDS operations should be activated to ensure EQD is completed before FPSO breaks through the physical limit.

It should be noted that the extreme sea conditions which happens with extremely low probability could cause catastrophic accident. If the drift-off scenario happens in the extreme sea conditions, the aforementioned operational plans incorporated with the provided predictions will possess higher risk than expectation. It is a limitation of the proposed methodology, as we assume that FPSO only be on service in normal sea state.

5. Conclusion

This study focuses on the prediction of the operational safety limits of dynamically positioned FPSO for the DAS system in the drift-off situation. A 3-phase probabilistic modelling methodology, which integrates the surrogate model and mechanical model with the probabilistic model, is proposed. The statistical distributions of operational safety limits are simulated by the successive approximation of the drift-off analysis for the FPSO and DAS coupling system. The accuracy of methodology is verified by a series of mathematical tests. The proposed methodology is successfully applied to the case study and reduced the computational cost without sacrificing accuracy or detail.

The structure integrity of the flexible jumper dominates the physical limit determination since the MBR failure of flexible jumper is the main cause for the structural failure of the DAS system. The MBR failure occurs at the connection between the flexible jumper and bend stiffener when FPSO drifts away from the DAS system to straighten the flexible jumper, whereas it occurs at the overhanging point of the flexible jumper when FPSO drifts close to the DAS system to bend the flexible jumper. For this reason, whether FPSO moving in the direction away from or close to the DAS system, there is a potential failure that requires the operators' attention.

In accordance with statistical results, most of operational safety limits are concentrated in two specific areas along the radius thus circling the safe moving range of FPSO, which is capable of guiding the DP operation in the drift-off scenario. This emphasizes the importance of the online monitoring of the FPSO position during the production operation. When the FPSO position is outside the safe moving range, a warning should be issued to inform operators that a drift-off might occur, and a series of preventive or contingency measures should be conducted in accordance with associated warning criteria.

The proposed methodology is a useful tool for the prediction of the critical position of dynamically positioned FPSO in real time. It visualizes the safe moving range of the FPSO, and thus provides ample time and information for operators to support drift-off decision-making. The study contributes to the safety control of the DP operations on floating production units. However, there still exist several limitations as following aspects:

- The mechanical model, surrogate model and probabilistic model should be re-established if the proposed methods are applied to different offshore sites.
- The extreme sea conditions which happen with extremely low probability can hardly be included in the statistical result. It is assumed that FPSO only be on service in normal sea state.
- The amplitudes of environmental loads are not included in the frequency contour of operational safety limit.

In the future work, actual field data will be utilized to be incorporated with the proposed methodology and further address these limitations.

Acknowledgements

The research is financially supported by the National Natural Science Foundation of China (No.51709041). In this challenging project, the authors appreciate the full support from Department of Marine Technology and AMOS center at NTNU.

Acronyms

ANN	Artificial Neural Network
CDF	Cumulative distribution function
DAS	Deepwater Artificial Seabed
DP	Dynamic positioning
EDS	Emergency disconnection sequence
EQD	Emergency quick disconnection
MBR	Minimum bend radius
MC	Monte Carlo
MCS	Maximum compression strain
MES	Maximum effective stress
MET	Maximum effective tension
PDF	Probability density function
QTF	Quadratic transfer function
RAO	Response amplitude operator
RBF	Radial basis function
SVC	Support Vector Classification
SVM	Support Vector Machine
SVR	Support Vector Regression
WSOG	Well Specific Operating Guidelines

References

[1] Zhen XW, Vinnem JE, Han Y, Peng CY, Yang X, Huang Y. New risk control mechanism for innovative deepwater artificial seabed system through online risk monitoring system. Applied Ocean Research 2020; 95.
[2] Lim F. Dry or wet trees in deepwater developments from a riser system perspective. Third ISOPE International Deep-Ocean Technology Symposium. Beijing, China 2009.
[3] Huang Y, Zhen XW, Zhang Q. Ultra-deepwater offshore oil-gas engineering developing system and mounting method. ZL201110439619.9. 20140409.
[4] Zhen XW, Huang Y. Parametric study on the behavior of an innovative subsurface tension leg platform in ultra-deep water. China Ocean Engineering 2017; 31(5): 589-597.
[5] Zhen XW, Moan T, Gao Z, Huang Y. Risk Assessment and Reduction for an Innovative Subsurface Well Completion System. Energies 2018; 11.
[6] Zhen XW, Han Y, Huang Y, Yao JJ, Wu JH. Analytical approach for the establishment of critical length criterion for the safe and economical design of the flexible jumper in deepwater applications. Applied Ocean Research 2018; 75: 193-200.
[7] Chen HB, Moan T, Verhoeven H. Safety of dynamic positioning operation on mobile offshore drilling units.

Reliability Engineering and System Safety 2007: 1072-1089.
[8] Chen HB, Abrahamsen B. Verification of DP safety barriers for offshore well intervention vessels. ASME 2009 28th International Conference on Ocean, Offshore and Arctic Engineering. 2009.
[9] Cruz DF, Fonseca DDR. WSOG and emergency disconnection guidelines. Offshore Technology Conference. Rio de Janeiro, Brazil 2017.
[10] DNV. Dynamic positioning systems - operation guidance. 2015.
[11] Teixeira FJR, Oshi AT, Tannuri EA. Drifting time of a standard drillship. Proceedings of the ASME 2014 33rd International Conference on Ocean, Offshore and Arctic Engineering. San Francisco, California, USA 2014.
[12] Rustad AM, Ervik AK, Sørensen AJ, Larsen CM. Increasing the operation window for drilling risers on DP vessels by monitoring riser angles. Proceedings of the ASME 2012 31st International Conference on Ocean, Offshore and Arctic Engineering. Rio de Janeiro, Brazil 2012.
[13] Bhalla K, Cao Y. Watch circle assessment of drilling risers during a drift-off and drive-off event of a dynamically positioned vessel. Dynamic Positioning Conference. Houston, Texas. USA 2005.
[14] Liu XQ, Chen GM, Chang YJ, Ji JQ, Fu JJ, Song Q. Drift-off warning limits for deepwater drilling platform/riser coupling system. Petroleum Exploration & Development Online 2016; 43(4): 701-707.
[15] Quigley C, Williams D. A revised methodology for the calculation of MODU watch circles. Proceedings of the ASME 2015 34th International Conference on Ocean, Offshore and Arctic Engineering. St. John's, Newfoundland, Canada 2015.
[16] Sullivan EO, Soles J, Dib M. Fully coupled EDS/drift-off analysis for a harsh environment, deepwater site. ASME International Conference on Offshore Mechanics & Arctic Engineering. 2004.
[17] Gjerde T, Chen HB. Probabilistic red limit study for mobile offshore drilling units. 33rd International Conference on Ocean, Offshore and Arctic Engineering. San Francisco 2014.
[18] Bhosekar A, Ierapetritou M. Advances in surrogate based modeling, feasibility analysis, and optimization: A review. Computers & Chemical Engineering 2018; 108: 250-267.
[19] Asher MJ, Croke BFW, Jakeman AJ, Peeters LJM. A review of surrogate models and their application to groundwater modeling. Water Resources Research 2015; 51(8): 5957-5973.
[20] Wang YY. Investigation of design wave parameters for Chinese coastal areas. China Ocean Engineering 1988; 2(4): 71-78.
[21] Ozay C, Celiktas MS. Statistical analysis of wind speed using two-parameter Weibull distribution in Alaçatı region. Energy Conversion and Management 2016; 121: 49-54.
[22] Liu M, Wu W, Tang D, Ma H, Naess A. Current profile analysis and extreme value prediction in the LH11-1 oil field of the South China Sea based on prototype monitoring. Ocean Engineering 2018; 153: 60-70.
[23] Chakrabarti SK. Hydrodynamics of offshore structures. Springer. 1987.
[24] Mookiah M R K, Hogg S, Macgillivray T J, Prathiba V, Pradeepa R, Mohan V, Anjana R M, Doney A S, Palmer C N A, Trucco E. A review of machine learning methods for retinal blood vessel segmentation and artery/vein classification. Medical Image Analysis 2021; 68: 101905.
[25] Ahmed K R, Akter S, Marandi A, Schüth C. A simple and robust wetland classification approach by using optical indices, unsupervised and supervised machine learning algorithms. Remote Sensing Applications: Society and Environment 2021; 23: 100569.
[26] Otchere D A, Arbi Ganat T O, Gholami R, Ridha S. Application of supervised machine learning paradigms in the prediction of petroleum reservoir properties: Comparative analysis of ANN and SVM models. Journal of Petroleum Science and Engineering 2021; 200: 108182.
[27] Rajasekaran S, Gayathri S, Lee T L. Support vector regression methodology for storm surge predictions. Ocean Engineering 2008; 35(16): 1578-1587.

[28] Tagliaferri F, Viola I M, Flay R G J. Wind direction forecasting with artificial neural networks and support vector machines. Ocean Engineering 2015; 97(15): 65-73.
[29] Oil & Gas UK. Tandem loading guidelines. 2014.
[30] API. Analysis, design, installation, and testing of safety systems for offshore production facilities. 2017.
[31] Zhen X W. Investigation on coupled motion and risk assessment of an innovative subsurface production. Dalian University of Technology, 2016.
[32] Huang Y, Zhen X W, Zhang Q, Wang W H. Optimum design and global analysis of flexible jumper for an innovative subsurface production system in ultra-deep water. China Ocean Engineering 2014; 28(2): 239-247.